The transient Dst electromagnetic induction signal at satellite altitudes for a realistic 3-D electrical conductivity in the crust and mantle

Jakub Velímský
Department of Geophysics, Charles University, Prague, Czech Republic

Mark E. Everett
Department of Geology and Geophysics, Texas A & M University, College Station, Texas, USA

Zdeněk Martinec
Kinematics and Dynamics of the Earth, GeoForschungsZentrum Potsdam, Germany

Received 26 November 2002; revised 3 February 2003; accepted 24 February 2003; published 1 April 2003.

[1] Magnetometer data from recent low-orbit satellite missions Ørsted and CHAMP offer an opportunity to improve our knowledge of electrical conductivity of the Earth's mantle. The forward modelling of electromagnetic induction (EM) is conventionally carried out in the frequency domain. We use a time-domain technique to study the electromagnetic response of a realistic 3-D electrical conductivity model based on seismic tomography and laboratory measurements. The model is excited by a Dst signal realistic in time evolution but simplified as spatial dipolar shape. The results show measurable response of simulated satellite time series to mid-mantle conductivity inhomogeneities. The interpretation of satellite magnetic data for the determination of 3-D mantle conductivity inhomogeneities will, however, require a more precise model of external ionospheric and magnetospheric currents. This can be obtained by simultaneous measurements by several satellites. *INDEX TERMS:* 1515 Geomagnetism and Paleomagnetism: Geomagnetic induction; 1555 Geomagnetism and Paleomagnetism: Time variations—diurnal to secular; 1594 Geomagnetism and Paleomagnetism: Instruments and techniques. **Citation:** Velímský, J., M. E. Everett, and Z. Martinec, The transient Dst electromagnetic induction signal at satellite altitudes for a realistic 3-D electrical conductivity in the crust and mantle, *Geophys. Res. Lett.*, *30*(7), 1355, doi:10.1029/2002GL016671, 2003.

1. Introduction

[2] Good spatial coverage of satellite magnetometer data, such as those obtained from the MAGSAT, Ørsted and CHAMP spacecrafts, offers an unprecedented opportunity to improve our knowledge of electrical conductivity in the Earth's mantle. The problem of electromagnetic induction in the mantle is traditionally solved in the frequency domain using land-based data [*Banks*, 1969; *Schultz and Larsen*, 1987, 1990]. Several methods have been developed recently to perform the forward problem of EM induction in a fully heterogeneous Earth taking into account the effect of lateral conductivity variations [*Kuvshinov and Pankratov*, 1994; *Everett and Schultz*, 1996; *Martinec*, 1999; *Uyeshima and Schultz*, 2000]. It is, however, inconvenient, to study the Earth's response to transient signals, such as magnetic storms, by the frequency-domain method. Moreover, the complicated spatio-temporal distribution of satellite data favors a time-domain approach. Various time-domain methods for the EM induction modelling in a heterogeneous sphere have recently been developed to compute a transient magnetic field induced in the Earth by an external magnetic source field [*Hamano*, 2002; Z. Martinec et al., submitted to *Geophysical Journal International*, 2002; J. Velímský and Z. Martinec, manuscript in preparation, 2003].

[3] In this paper, we consider a realistic crust and upper-mantle conductivity model based on laboratory measurements and seismic tomography. This model is excited by a transient Dst signal taken from the period 1979–1980. We will study the sensitivity of the EM response observed at satellite altitudes to lateral conductivity variations in the upper mantle, which are overlain by the near-surface conductivity in homogeneities characterizing the ocean, continent and sea-shelf distribution.

2. Time-Domain Approach

[4] A detailed description of the time-domain method of EM induction in a laterally inhomogeneous sphere will be given elsewhere. Here we only present a brief outline of the method. The governing equation of electromagnetic induction, that is the magnetic diffusion equation,

$$\mu_0 \frac{\partial \mathbf{B}}{\partial t} + \mathrm{curl}\left(\frac{1}{\sigma}\mathrm{curl}\mathbf{B}\right) = 0, \qquad (1)$$

is first reformulated in the weak sense. The magnetic induction vector **B** is parameterized by vector spherical harmonics in the angular direction and by piecewise linear finite elements in the radial direction. The conductivity σ is spanned by piecewise constant functions in the radial direction. In the angular direction, σ is prescribed at grid points equidistantly spaced in longitude φ and at the roots of Legendre polynomials in colatitude ϑ. A semi-implicit Euler scheme is applied to time integration. The terms containing the radial part of the conductivity are treated implicitly in time, while the terms depending on the lateral part of the conductivity are computed explicitly by making use of the solution from the previous time step. For an acceptable global spatial resolution (the cut-off degree of spherical

Copyright 2003 by the American Geophysical Union.
0094-8276/03/2002GL016671$05.00

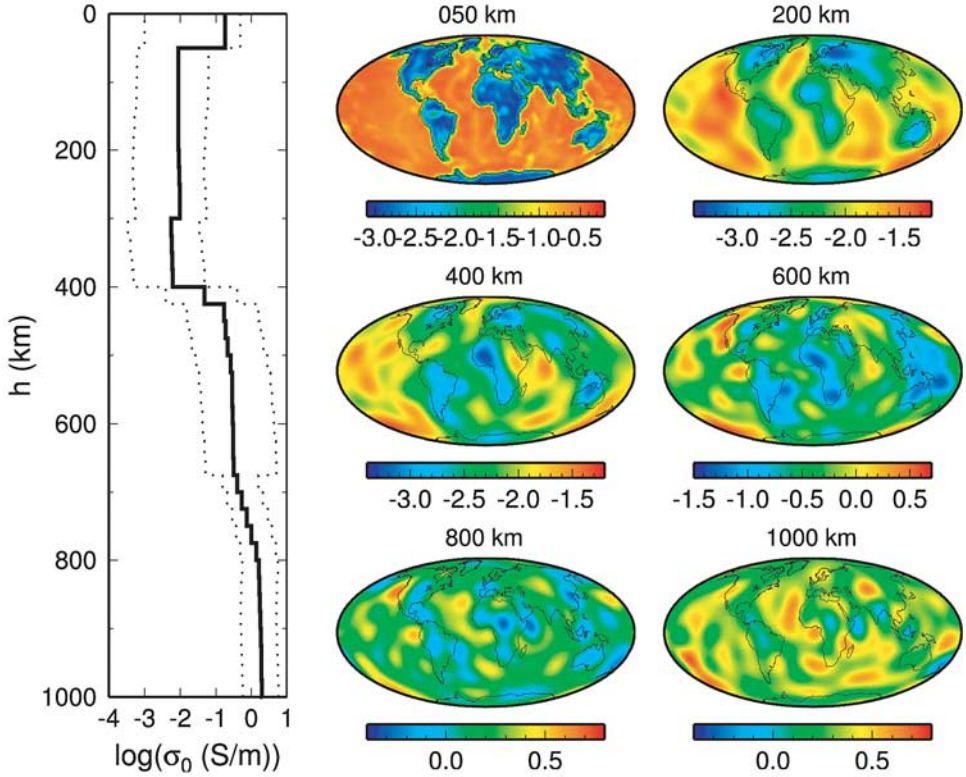

Figure 1. 3-D conductivity model in the crust, upper and mid-mantle. The solid line in the left panel shows the 1-D profile based on laboratory measurements [*Xu et al.*, 2000]. Lateral variations are confined to the interval shown by dotted lines. The first color map on the right shows the conductivity obtained from the surface conductance map for a uniform depth of 50 km. The following cross-sections sample the tomography-derived conductivity at depths of 200, 400, 600, 800, and 1000 km. All scale bars are in units of log(σ (S/m)).

harmonic expansion is 40, the number of gridpoints in radial direction is 100), one timestep of a solution requires about 15 s of CPU time on a 500 MHz PC.

[5] The method has been successfully tested with respect to semi-analytical solutions for conductivity models consisting of multiply nested homogeneous spheres [*Martinec*, 1998]. Various models of exciting external field have been applied, including harmonic signals of periods ranging from 2 to 240 days, a simple analytical model of a geomagnetic storm of the form $t\exp(-at)$, and pulses 4 to 24 hours long. Here, we will consider a more complex Dst exciting signal.

3. Conductivity Model

[6] We construct a 3-D conductivity model based on three data sources. The contrasts between the highly conductive oceans water, resistive continents, and intermediate shelves and marine sediments are treated using the surface conductance map constructed by *Everett et al.* [2003]. The conductance is converted to conductivity using a layer with constant thickness of 50 km (see Figure 1).

[7] The conductivity in the upper and lower mantle is based on the 1-D conductivity model derived by *Xu et al.* [2000] from laboratory measurements, combined with the seismic tomography model SKS12WM13 by *Liu et al.* [1994]. Although the shear-wave velocity and electrical conductivity have different sensitivity to various physical and chemical properties of the mantle, the positive correlation between the conductor depths and velocity perturbations obtained by *Tarits* [1994] supports the basic correspondence between the fast, cold, and resistive mantle contrasting to the slow, hot, and conductive areas.

[8] Approximating the relation between electrical conductivity and shear-wave velocity variation δV by an exponential function, the conductivity σ at depth h, colatitude ϑ, and longitude φ is

$$\sigma(h,\vartheta,\varphi) = \sigma_0(h) f(h)^{-\frac{\delta V(h,\vartheta,\varphi)}{\delta V_M(h) - \delta V_m(h)}}, \qquad (2)$$

where $\delta V_M(h)$ and $\delta V_m(h)$ are respectively the maximum and minimum lateral seismic-velocity variations at depth h taken from SKS12WM13, and $\sigma_0(h)$ is the 1-D conductivity model by *Xu et al.* [2000]. The base $f(h)$, which is the ratio of the maximum to minimum conductivity in each layer, is set to 100 in the upper mantle and to 10 in the lower mantle [*Shankland et al.*, 1993]. Finally, a homogeneous core with conductivity 10 000 S/m is assumed.

[9] In order to evaluate the compatibility of the 3-D conductivity model with surface geomagnetic data, the Schmucker C-responses are computed in the frequency range 0.01 to 0.2 cpd using the spectral-finite element code by *Martinec* [1999]. Figure 2 shows them compared with 22 local 1-D responses from the dataset by *Schultz and Larsen* [1987]. The agreement between the synthetic and observed data at individual stations is highly variable with the χ^2 misfit ranging from 19.03 up to 1409.18. Addition of the lateral conductivity variations according to (2) to the 1-D

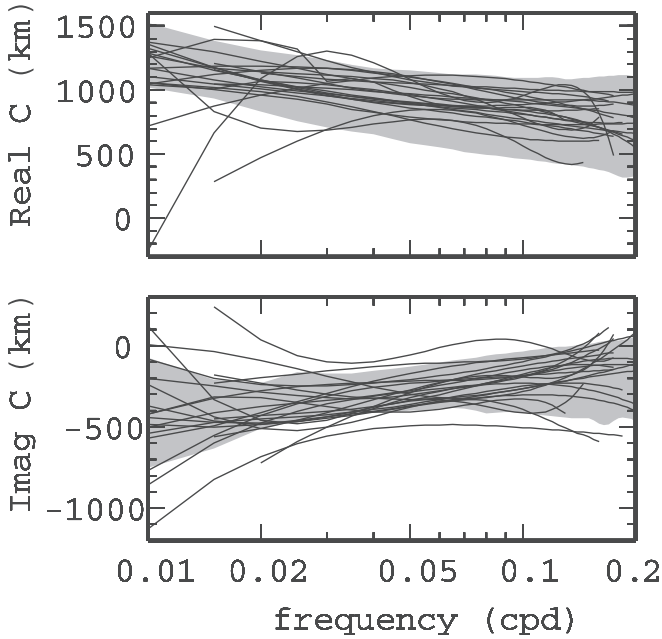

Figure 2. The Schmucker *C*-responses generated by the 3-D conductivity model. At middle geomagnetic latitudes, $25° \leq |\lambda_d| \leq 65°$, these are limited to the areas shown by grey shading. Local 1-D responses computed by *Schultz and Larsen* [1987] for 22 ground stations are stacked over using solid lines.

profile $\sigma_0(h)$ improved the fit to the observed *C*-responses at 13 stations. At the remaining 9 stations the misfit obtained for the 3-D model is larger than for the 1-D model. These results must be interpreted cautiously, since the 3-D conductivity model does not comply with the assumption of local 1-D structure used in the processing of local responses. In general, the model shows a degree of lateral heterogeneity appropriate to the observed responses, although the particular conductivity structures in the model may differ from those required by the surface data.

4. Exciting Field

[10] We excite the conductivity model specified in the previous section by a transient, axisymmetric ring current. This is a first-order approximation of the spatial distribution of Dst currents [*Daglis and Kozyra*, 2002]. Assuming a P_{10} geometry for the exciting field in the geomagnetic coordinate system, the dipolar coefficient of the external magnetic potential $G_{10}^{(e)}$ can be derived from the Dst index (downloaded from the WDC-C2 Kyoto Dst index service, http://swdcdb.kugi.kyoto-u.ac.jp/dstdir/), by a simple scaling formula,

$$G_{10}^{(e)}(t) = -\sqrt{\frac{4\pi}{3}}\frac{Dst(t)}{1+Q_1}, \qquad (3)$$

where $Q_1 = 0.27$ is the global estimate of the internal to external fields ratio [*Langel and Estes*, 1985].

[11] Figure 3 shows the time evolution of $G_{10}^{(e)}$ during three successive magnetic storms in January and February, 1980. At this epoch the solution has already evolved for more than 1900 h to ensure that the presented results are not biased by the choice of initial value of the magnetic field, which is an inherent feature of the time-domain method.

5. Results

[12] In the case of an azimuthally symmetric external excitation and a 1-D conductivity model, the longitudinal component B_φ vanishes. Therefore, B_φ may serve as a tool to study the effect of lateral conductivity variations on the EM induction response. Figure 4 shows the snapshots of B_φ computed at 400 km altitude, which is typical of low-orbit satellites.

[13] The largest magnetic anomalies, up to 1.2 nT in B_φ and up to 2.2 nT in non-dipolar parts of B_r and B_ϑ computed at satellite altitude can be assigned to the resistive areas in the transition zone below South America, Africa, and the western Pacific. On the other hand, the signal due to the large positive anomaly at 200 km depth below the eastern Pacific is weaker. The induced field shows similar spatial structure for different storms with the largest amplitude corresponding to the most severe storm. This is not surprising, since the imposed inducing field has the same dipolar spatial structure all the time. Note, that in the last snapshot in Figure 4, the small positive *Dst* index (i.e., negative $G_{10}^{(e)}$) yields change of the sign also in the induced anomalous field.

6. Discussion

[14] Our simulation shows that the EM response of the realistic conductivity model to intense transient changes in the ring-current system is detectable by a low-orbit satellite magnetometer. The magnitude of the signal induced by the highly heterogeneous oceanic/continental layer is less than 10% smaller than that of the mid-mantle conductivity heterogeneities. This is in agreement with the results of previous synthetic studies carried out in the frequency domain using surface observations [*Weiss and Everett*, 1998].

[15] Since the period we covered coincides with the MAGSAT mission, direct comparison of the results is advisable. S. Constable and C. Constable (manuscript in preparation, http://mahi.ucsd.edu/Steve/MDAT/, 2001) isolated the Dst signal from MAGSAT data, and showed that

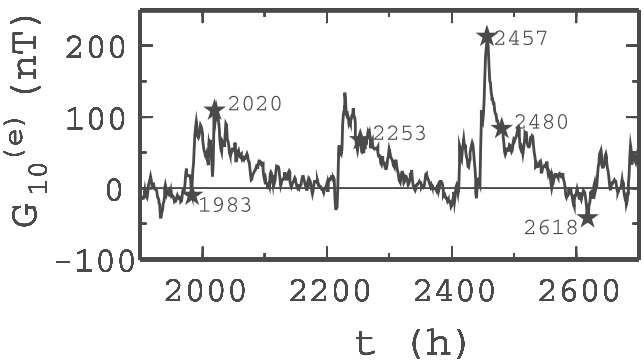

Figure 3. The coefficient $G_{10}^{(e)}$ of the external excitation field. Time $t = 0$ corresponds to Nov. 5, 1979, 0:00 UT, the displayed interval spans over three successive storms occurring between Jan. 24 and Feb. 27, 1980. Stars mark the epochs shown in Figure 4.

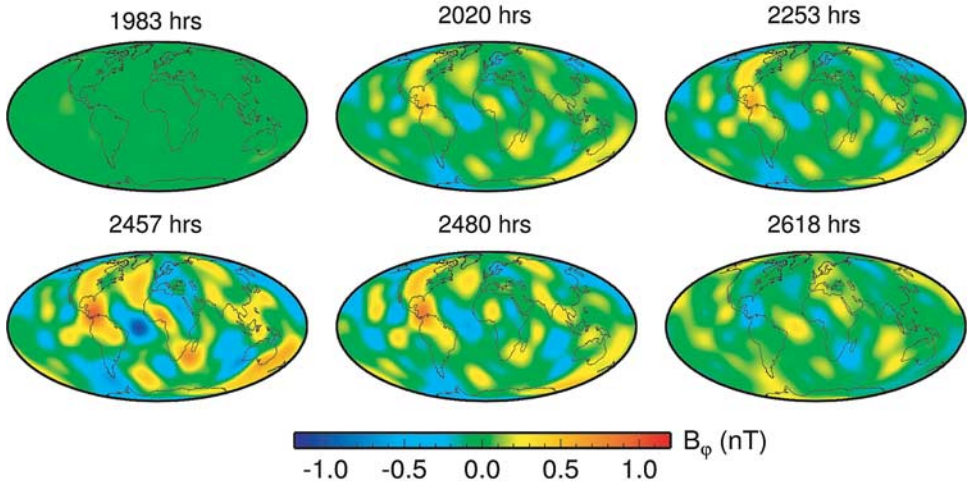

Figure 4. The computed B_ϕ component at satellite altitude 400 km. Snapshot at t = 1983 h corresponds to the onset of the magnetic storm. At t = 2020, and 2457 h the storm culminate, and t = 2253, 2480, and 2618 h sample the recovery phases. The time snapshots are marked in Figure 3

after fitting the P_{10} model for individual satellite passes, the RMS residuals are 5 to 6 nT for B_r, and B_ϑ components, and up to 11 nT in the B_φ component for the ascending passes of the spacecraft. These residuals represent, beside possible remnants of non-Dst signals, a combined effect of non-P_{10} external sources, and lateral conductivity variations. In order to distinguish between these two components and to interpret satellite magnetic data in terms of laterally varying conductivity models, a more accurate model of the temporal and spatial variations of the external excitation field will be necessary. The combination of satellite data from several satellites and land-based measurements should allow to go beyond the simple P_{10} excitation model. The time resolution needed to resolve rapid changes of the external field is of the order of a typical orbital period of a satellite (∼1 h).

[16] **Acknowledgments.** The research presented in this paper was supported by grant No. 205/00/1367 of the Grant Agency of the Czech Republic, Charles University grant No. 238/2001/B-GEO/MFF, National Science Foundation EAR-0087643 and by the U.S.-Czech Scientific Exchange Program of the National Research Council COBASE. We thank C.J. Weiss and an anonymous reviewer for helpful comments.

References

Banks, R. J., Geomagnetic variations and the electrical conductivity of the upper mantle, *Geophys. J. R. Astron. Soc.*, *17*, 457–487, 1969.

Daglis, I. A., and J. U. Kozyra, Outstanding issues of ring current dynamics, *J. Atmos. Solar Terr. Phys.*, *64*, 253–264, 2002.

Everett, M. E., and A. Schultz, Geomagnetic induction in a heterogeneous sphere: Azimuthally symmetric test computations and the response of an undulating 660-km discontinuity, *J. Geophys. Res.*, *101*, 2765–2783, 1996.

Everett, M. E., S. Constable, and C. Constable, Effects of near-surface conductance on global satellite induction responses, *Geophys. J. Int.*, *153*, 277–286, 2003.

Hamano, Y., A new time-domain approach for the electromagnetic induction problem in a three-dimensional heterogeneous Earth, *Geophys. J. Int.*, *150*, 753–769, 2002.

Kuvshinov, A. V., and O. V. Pankratov, Electromagnetic induction in a spherical Earth with inhomogeneous conducting mantle: Thin sheet forward problem, paper presented at 12th Workshop on Electromagnetic Induction in the Earth, Univ. de Bretagne Occidentale, Brest, France, 1994.

Langel, R. A., and R. H. Estes, Large-scale, near-field magnetic fields from external sources and the corresponding induced internal field, *J. Geophys. Res.*, *90*, 2487–2494, 1985.

Liu, X.-F., W.-J. Su, and A. M. Dziewonski, Improved resolution of the lower-most mantle shear wave velocity structure obtained using SKS-S data, *Eos Trans. AGU*, *75*(16), 232, Spring Meet. Suppl., 1994.

Martinec, Z., Geomagnetic induction in multiple eccentrically nested spheres, *Geophys. J. Int.*, *132*, 96–110, 1998.

Martinec, Z., Spectral-finite element approach to three-dimensional electromagnetic induction in a spherical Earth, *Geophys. J. Int.*, *136*, 229–250, 1999.

Schultz, A., and J. Larsen, On the electrical conductivity of the mid mantle—I. Calculation of equivalent scalar magnetotelluric response functions, *Geophys. J. R. Astron. Soc.*, *88*, 733–761, 1987.

Schultz, A., and J. Larsen, On the electrical conductivity of the mid mantle: II. Delineation of heterogeneity by application of extremal inverse solutions, *Geophys. J. Int.*, *101*, 565–580, 1990.

Shankland, T. J., J. Peyronneau, and J. P. Poirier, Electrical conductivity of the Earth's lower mantle, *Nature*, *366*, 453–455, 1993.

Tarits, P., Electromagnetic studies of global geodynamic processes, *Surv. Geophys.*, *15*, 209–238, 1994.

Uyeshima, M., and A. Schultz, Geoelectromagnetic induction in a heterogeneous sphere: A new three-dimensional forward solver using a conservative staggered-grid finite difference method, *Geophys. J. Int.*, *140*, 636–650, 2000.

Weiss, C. J., and M. E. Everett, Geomagnetic induction in a heterogeneous sphere: Fully three-dimensional test computations and the response of a realistic distribution of oceans and continents, *Geophys. J. Int.*, *135*, 650–662, 1998.

Xu, Y., T. J. Shankland, and B. T. Poe, Laboratory-based electrical conductivity in the Earth's mantle, *J. Geophys. Res.*, *105*, 27,865–27,875, 2000.

M. E. Everett, Department of Geology and Geophysics, Texas A & M University, College Station, TX 77843, USA.

J. Velímský, Department of Geophysics, Charles University, Faculty of Mathematics and Physics, V Holešovičkách 2, 18000 Prague, Czech Republic. (jakub.velimsky@mff.cuni.cz)

Z. Martinec, GeoForschungsZentrum Potsdam, Div.1, Kinematics and Dynamics of the Earth, Telegrafenberg, D-14473 Potsdam, Germany.